Quantum Monte Carlo study of superradiant supersolid of light in the extended Jaynes-Cummings-Hubbard model

Huanhuan Wei,[1] Jie Zhang,[1,2,*] Sebastian Greschner,[3] Tony C Scott,[4] and Wanzhou Zhang[1,†]

[1]*College of Physics and Optoelectronics, Taiyuan University of Technology, Shanxi 030024, China*
[2]*State Key Laboratory of Quantum Optics and Quantum Optics Devices, Shanxi Taiyuan 030024, Shanxi, China*
[3]*Department of Quantum Matter Physics, University of Geneva, 1211 Geneva, Switzerland*
[4]*Institut für Physikalische Chemie, RWTH Aachen University, D-52056 Aachen, Germany*

(Received 5 October 2020; revised 8 February 2021; accepted 9 February 2021; published 3 May 2021)

Searching for and investigating supersolids is a long-term outstanding problem in physics. In addition to the solid element ^{4}He and cold atoms as potential candidates for the supersolid, the quantum system of light realized by circuit quantum electrodynamics is also a promising platform. In this paper, we propose a supersolid phase, i.e., a superradiant supersolid of light, where superradiant, superfluid, and solid orders coexist. We theoretically simulate the extended Jaynes-Cummings-Hubbard model describing the circuit quantum electrodynamics systems, mainly by the large-scale worm quantum Monte Carlo method, and find that a superradiant supersolid phase exists on triangular lattices due to the antiferromagnetic correlation between photons via light-atom coupling. We also confirm that the previous supersolid of light given by Bujnowski *et al.* [Phys. Rev. A **90**, 043801 (2014)] is not stable. The phase transition between our superradiant supersolid phase and the superradiant solid phase can be continuous (first order) and above (below) the "symmetry point." This is not the same as the pure Bose-Hubbard model on triangular lattices. The results herein could help in the search for a new superradiant supersolid phase in circuit quantum electrodynamic experiments and other light-matter coupling systems.

DOI: 10.1103/PhysRevB.103.184501

I. INTRODUCTION

The supersolid (SS) phase is one of the most paradoxical predictions of quantum theory and has attracted great interest for decades [1–4]. It can simultaneously possess both superfluid and solid features, although these characteristics are always mutually exclusive. This extraordinary phase breaks the phase invariance of the superfluid and the continuous translational invariance [5]. It was first assumed that it might emerge in solid ^{4}He in 1970 [3]. However, after decades of theoretical and experimental efforts [6], proof of a SS phase in solid ^{4}He is still elusive [7–10]. Recently, a breakthrough occurred in ultracold quantum matters, where two groups declared observations of the SS phase with cavity-mediated interactions [11] and spin-orbit coupling [12] and another three independent groups reported the generation of the SS phase through dipolar interactions [13–15]. However, the validity of the claim that it has been observed preliminarily in cold atoms needs better confirmation [16].

Apart from the ^{4}He and cold-atom experiments, the quantum fluid of light as another quantum simulation candidate has been developed extensively [17]. It is universally known that light obeys the wave-particle duality, and it can be defined as a collection of photons generated by a light source which freely spread until absorbed. If frequent collisions between photons can occur, this might lead to collective fluidlike behavior in the many-photon system, where the photon-photon interaction can be implemented by light-matter coupling. One of the promising media for the study of quantum fluids of light is the circuit quantum electrodynamics (CQED) system, which can be realized by an array of coupled cavities based on superconducting Josephson junctions [18,19]. The tight confinement of microwaves on a chip naturally results in an extremely strong atom-photon coupling, offering a new platform for SS experiments [20].

The CQED system can theoretically be described by the Jaynes-Cummings-Hubbard (JCH) model [21–25], where many interesting phenomena in light-matter coupling systems have been predicted [26–30], such as superfluid-insulator transitions of polaritons [26], fractional quantum Hall physics [31], quantum transport [32], quantum-state transmission [33], on-site disorder [28,34], etc. However, exploration of the physics of the JCH model on lattices is still a challenge, even when using reliable large-scale simulations with the quantum Monte Carlo (QMC) method. For example, the nature of the superfluid-insulator transition was misunderstood, and was found to have three-dimensional XY universality, as reported by Hohenadler *et al.* [35]. At the same time, the photon-atom coupling leads to a superradiant superfluid [36] or superradiant solid [37] in Bose systems and the superradiation-normal phase transition in a Fermi gas [38] trapped in a single cavity.

Naturally, the following question arises: by extending the single-cavity case to the lattices of a cavity array with various geometries, can one expect the JCH model to possess a new phase, superradiant SS (SRSS)? SRSS is expected to have superradiation, superfluid, and solid orders simultaneously.

*Corresponding author: zhangjie01@tyut.edu.cn
†Corresponding author: zhangwanzhou@tyut.edu.cn

The basic issue of this paper is to explore whether or not the SRSS phase exists, how the phase transition properties are different from the pure Bose-Hubbard (BH) model [39], and how to realize the SRSS phase both theoretically and experimentally.

Reference [40] showed the SS phase of light in the JCH model by using the cluster mean-field (CMF) method [41–43]. Given that the CMF method ignores quantum fluctuations, the authors of this reference expected a reliable method to vindicate their findings. Two of the authors of Ref. [44] used the density matrix renormalization group method [45,46] to give an interesting paired SS phase for the JCH model on different ladders. Furthermore, on two-dimensional triangular lattices, they presented a preliminary phase diagram also using the CMF method. Although the cluster size has up to 36 sites, we still need more reliable methods to confirm the stability of the SS phase. At any rate, there are still unsolved problems, including the unmentioned superradiant properties of the SS phase.

To address these questions, we first map the problem to a BH model [39] on a two-layer geometry, where one layer describes the photon and the other describes the atom excitation [47]. We then use the large-scale worm QMC method [48–51], to simulate the model in various geometries. We find that for bipartite lattices, there is no SS phase in the extended JCH model. The SS phase previously predicted by the CMF method [40] is not stable; that is, the transition between the solid phase and the superfluid phase is actually of first order with obvious jumping of the order parameters such as superfluid stiffness and structural factors with larger lattices. To search for a SRSS phase of light, the JCH model on the two-dimensional triangular lattices is studied, and a stable SRSS phase of light is found. We also use the compressibility of photons and atom excitation to analyze the superradiant properties of the SS phase. The phase transition type of the SRSS phase to the solid phase is not completely the same as the ones from the pure BH model, especially on triangular lattices. For example, the (1/3)-filled superradiant solid (SII) to the SRSS phase can be first order, and this has not been reported, as discussed in detail in Sec. IV.

The outline of this paper is as follows: Section II introduces the model, its difference from the pure BH model, the methods, and the measured quantities. Section III shows the results on bipartite lattices such as one-dimensional (1D) and two-dimensional (2D) square lattices. Section IV gives the results of the JCH models on triangular lattices. Section V shows how the experimental realization of the model is made and the expression of its parameters. Conclusions are made in Sec. VI. In Appendix A, a one-dimensional chain and a square lattice are illustrated. In Appendixes B and C, we compare the results from both the WQMC and exact diagonalization (ED) methods and also show the details of the CMF methods.

II. MODEL, METHODS, AND THE MEASURED QUANTITIES

A. Model and its mapping

The extended JCH model includes a repulsion between excitations of the adjacent cavities with strength V, which is different from the atom-atom repulsion interaction. The model has many cavities, and each cavity can be considered a site in the lattices. In each cavity, there is a two-level atom. Simultaneously, photon tunneling between cavities is considered.

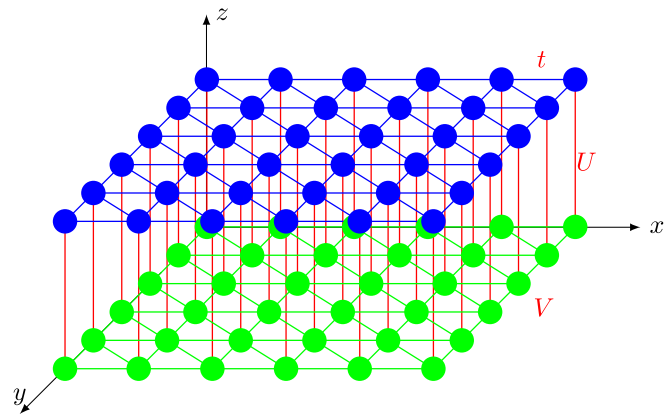

FIG. 1. The mapped two-layer triangular lattices for the JCH model, where the top and bottom layers are denoted as photon and atom layers, respectively. The hopping of the photons t, atom-photon coupling U, and interactions between atom excitations V are labeled. A one-dimensional chain and a square lattice are illustrated in Appendix A.

To simulate the model conveniently, the model is mapped onto a pure BH model in two-layer geometries, e.g., two-layer triangular lattices, as shown in Fig. 1, where the top layer and bottom layer describe the state of the photon and the level of the atom, respectively. For a specific site $\mathbf{r} = (x, y)$, if the two-level atom sits in the ground state, then the state at $(x, y, z = 1)$ should be empty, and the excited state should be occupied. Similarly, the state at $(x, y, z = 2)$ describes the photon number in each cavity.

In comparison to the pure BH model, the interaction and hopping between layers are different. In the photon layer, only photon hopping without repulsion exists, and in the atom layer, only repulsion without the hopping term exists. The extended JCH Hamiltonian is defined as

$$H = \sum_i \left(H_i^{\mathrm{JC}} - \mu n_i\right) - t \sum_{\langle i,j\rangle} (a_i^\dagger a_j + \mathrm{H.c.}) + \sum_{\langle \mathrm{i,j}\rangle} \mathrm{V n_i^\sigma n_j^\sigma}, \tag{1}$$

where the total number of excitations is $\rho \equiv \sum_i n_i = \sum_i (n_i^\sigma + n_i^a)$, μ is the chemical potential, $a_i^\dagger$ and a_i are, respectively, the photon creation and annihilation operators at lattice site i, and the term $(a_i^\dagger a_j)$ with strength t represents the photon hopping between cavities. The on-site coupling between the photons and the atom on each site i can be described by the JC Hamiltonian H_i^{JC},

$$H_i^{\mathrm{JC}} = \omega n_i^a + \varepsilon n_i^\sigma + U(a_i^\dagger \sigma_i + a_i \sigma_i^\dagger), \tag{2}$$

where U is the atom-photon coupling strength and represents the tunneling between layers, ω is the frequency of the model of the photon creation and annihilation operators at lattice site i, and ε is the transition frequency between two energy levels. For simplicity, we make the restriction $\omega = \varepsilon = 0$. Operators $n_i^a = a_i^\dagger a_i$ and $n_i^\sigma = \sigma_i^\dagger \sigma_i$ are the photon number and the number of excitations of the atomic levels, respectively. The Pauli

matrices $\sigma_i^\dagger$ (σ_i) represent the raising (lowering) operators for the atom levels.

B. Differences from the BH model

In 1970 [52] and 1973 [53], a lattice Hamiltonian was theoretically applied to investigate SS. In recent decades, experiments on optical lattices in cold-atom systems make it possible to synthesize and investigate the SS phase in the laboratory, where the BH models became the most popular model for studying SS. Exploration of the BH model and its variations is quite extensive. This includes the two-component BH model [54–56], the paired BH model [57–62], and the BH model with next-nearest-neighbor interactions [63,64]. Other efforts, such as the Bose-Fermi mixture [65,66], the fermion system [67], the spin system [68,69], spin-orbit coupled systems [70], and dipolar bosons [71], are also attractive possibilities.

As discussed in the last section and described in Fig. 1, the JCH can be mapped to the unconventional BH model on two layers. In the first layer, there is no interaction term, while in the second layer there is no tunneling between adjacent sites. At the same time, there is tunneling between layers. However, the SRSS phase can emerge in the both upper and bottom layers through the interaction induced by the atom-photon coupling.

C. Methods and the quantities measured

The conclusive results are mainly obtained by the WQMC method, and the details can be found in Refs. [48–51]. Here, in the real simulations, the inverse temperature $\beta = 1/k_bT$ takes larger values, namely, $\beta = 100,\ 500,\ \ldots,\ 1500$, to allow the systems to converge to the ground state.

We have tried a stochastic series expansion QMC method [72,73]. However, due to local atom-photon coupling and the no-hopping term between each atom layer, the updating efficiency is very slow in low-temperature regimes. The needed quantities for the WQMC algorithm are as follows:

(I) The local photon density $\rho_i^a = \langle n_i^a \rangle$, and local atom excitation $\rho_i^\sigma = \langle n_i^\sigma \rangle$.

(II) The superfluid stiffness [74]

$$\rho_s = \sum_{r=1}^{d} \frac{L^{2-d}\langle W_r\rangle^2}{2d\beta t}, \tag{3}$$

where W_r is the winding number of the photons in the upper layer in the x or y direction. The stiffness characterizes the nondiagonal long range order of the system.

(III) The structural factor of photons is given by

$$S(\mathbf{Q})/N = \langle \rho_{\mathbf{Q}} \rho_{\mathbf{Q}}^\dagger \rangle, \tag{4}$$

where $\rho_{\mathbf{Q}} = (1/N)\sum_i n_i^a \exp(i\mathbf{Q}\mathbf{r}_i)$, $N = L \times L$ is the total number of physical sites for 2D systems, and $N = L$ for 1D systems. For a one-dimensional lattice, the wave vector is at $\mathbf{Q} = (\pi, 0)$. In real space, the density of excitation obeys configurations of the form $(101010\cdots)$ or $(010101\cdots)$. The phase here is called the solid I (SI) phase. For square lattices, the solid with $\mathbf{Q} = (\pi, \pi)$ is also called the SI phase.

For two-dimensional triangular lattices, the wave vector is at $\mathbf{Q} = (4\pi/3, 0)$, and excitation densities obey configurations of the form $(001001\cdots)$ or $(110110\cdots)$. The densities are $1/3$ and $2/3$ and are called the SII phase and SIII phase, respectively.

(IV) The momentum distribution is given by

$$n(\mathbf{Q}) = \frac{1}{N}\sum_{j,j'} \langle a_j^\dagger a_{j'} \rangle e^{i\mathbf{Q}(\mathbf{r}_j - \mathbf{r}_{j'})}. \tag{5}$$

(V) The compressibility of photons and atom excitation is defined as [37]

$$\kappa_T^{a(\sigma)} = \frac{\beta}{N}\langle (N^{a(\sigma)})^2 \rangle - \langle N^{a(\sigma)} \rangle^2, \tag{6}$$

where $N^{a(\sigma)} = \sum n_i^{a(\sigma)}$. The two terms can be extracted from the structure factor $S(qx, qy)$ at $qx = 0$ and $qy = 0$ and the average of number of photons (or atom excitations). The compressibility is used to identify superradiation, which is a collection of photons and atom excitations, and is directly related to the fluctuation of the total number of photons (atom excitations).

The quantities ρ, $S(\pi)/L$, and energy density E are calculated by ED and the WQMC methods. The results are consistent with each other and are shown in Appendix B. In the SRSS phase, $S(\mathbf{Q})/N$, $\rho_s^{x(y)}$, and $\kappa_T^{a(\sigma)}$ are nonzero in the thermodynamic limit. Moreover, the global phase diagram is plotted with $\Psi = \langle a \rangle$ in the CMF frame, as illustrated in Appendix C for completeness.

III. RESULTS FOR THE JCH MODEL ON BIPARTITE LATTICES

In this section, we focus on the results of the JCH models on both the 1D and square lattices.

A. Phase diagram and details of the 1D JCH model

For the 1D hard-core extended JCH model, the maximum number of photons is restricted to be one in each cavity. It is well known that the number of photons is not fixed in a grand-canonical ensemble [35]. Therefore, the soft-core photon system has been checked, and the physics does not change [44].

Figure 2 shows the CMF phase diagram [41–43], which contains the empty, SI, SS, superfluid (SF) and Mott insulator (MI) phases, by plotting Ψ in the plane $(t/U, \mu/U)$.

As discussed in Ref. [24], in the regime at a large hopping t/U, the ground state energy becomes negative and can be made arbitrarily small by increasing the total number of excitations. Here, since the maximum number of photons is fixed, the SF phase remains stable.

The green dashed line labels the position scanning by WQMC, and the red triangles are the phase boundaries given by the WQMC method. In Figs. 3(a)–3(c), the results of excitation densities ρ, the structural factor $S(\pi)/L$ of photons, and superfluid stiffness ρ_s^x are shown as a function of μ/U with system sizes up to $L = 96$ and a thermodynamic limit $L = \infty$ with the sufficiently low temperature $\beta = 1500$.

In the interval $-0.933 < \mu/U < -0.903$, three quantities have platforms with $S(\pi/L) \neq 0$ and $\rho_s^x = 0$, and the phases

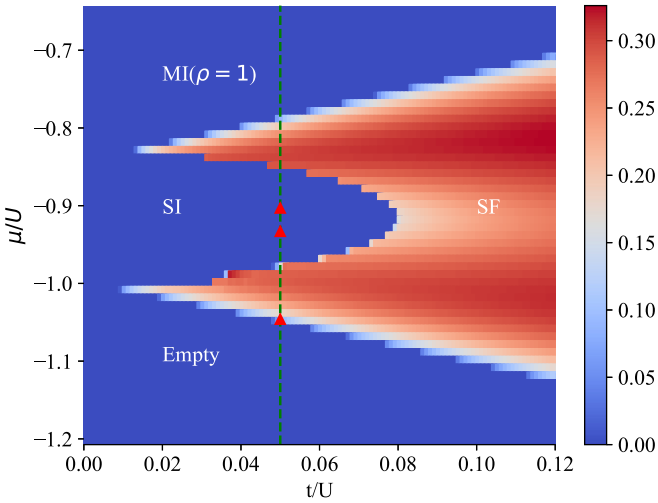

FIG. 2. Phase diagram and a detailed description of Ψ for the 1D hard-core extended JCH model with $V/U = 0.4$ by the CMF method. The green dashed line labels the position scanning, and the red triangles are the phase boundaries given by the WQMC method.

are all SI. By doping vacancies or excitations on the SI phase, $S(\pi)/L$ converges to zero, and ρ_s^x becomes nonzero at $L \to \infty$. The behavior of the jump at those two ends of the platform represents clear first-order transitions between the SF and SI phases, and obviously, no SS phase exists. The SS

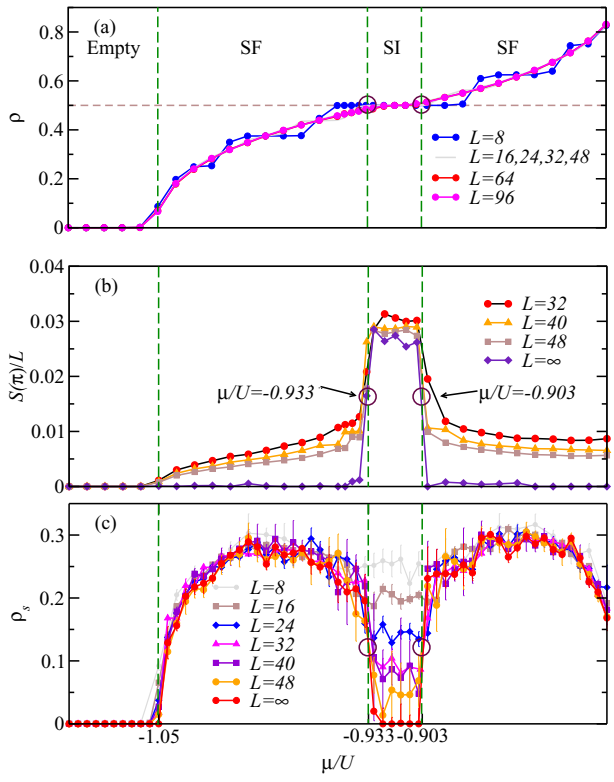

FIG. 3. Simulation results from WQMC method for (a) excitation densities ρ (up to $L = 96$), (b) structural factors $S(\pi)/L$, and (c) superfluid stiffness ρ_s as a function of μ/U with system sizes $L = 8$, 16, 24, 32, 40, 48, and ∞ at parameters $V/U = 0.4$ and $t/U = 0.05$.

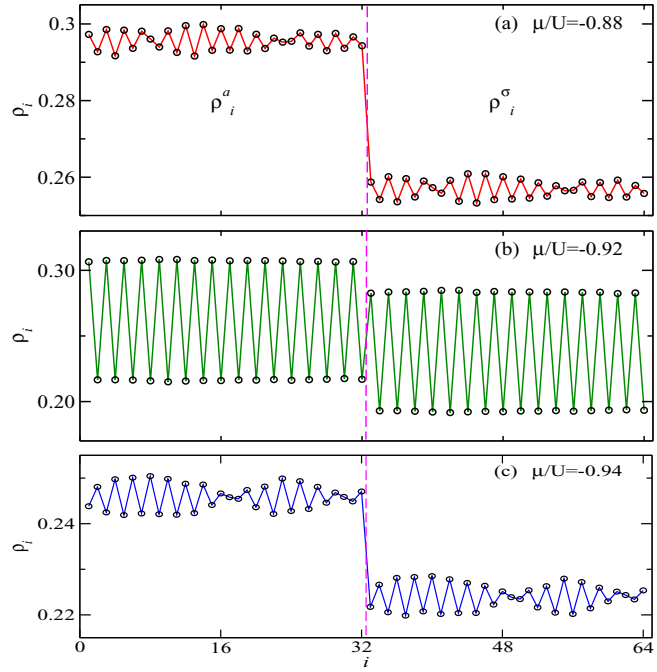

FIG. 4. Local photon density ρ_i^a, local atom excitation density ρ_i^σ, and solitonic signature in the upper and bottom layers as a function of position i with $V/U = 0.4$ and $t/U = 0.05$. (a) $\mu/U = -0.88$, with on-site excitation density $\rho > 1/2$. (b) $\mu/U = -0.92$, with $\rho = 1/2$. (c) $\mu/U = -0.94$, with $\rho < 1/2$.

phase is unstable against the phase separation, similar to the pure BH models [75–78]. Furthermore, the phase transition points from the empty phase to the SF phase. The predictions of the CMF and WQMC methods are completely the same at $\mu/U = -1.05$.

B. Beats or solitons in the SF phase

In the regime $-1.05 < \mu/U < -0.933$, $S(\pi)/L$ is not zero for a finite system size [see Fig. 3(b)]. To further understand $S(\pi)/L$, we illustrate the local photon densities ρ_i^a and the local atom excitation density ρ_i^σ as a function of position i under different values of chemical potential μ in Fig. 4. The commensurate density distribution arises in Fig. 4(b), which confirms the periodic ground state long-range crystalline order in the solid phase. The on-site excitation density in the solid phase is calculated to be $\rho = 1/2$, including both photons and atoms. Therefore, the local photon density ρ_i^a in the upper layer oscillates between 0.19 and 0.31 with the average value being 0.25.

As shown in Figs. 4(a) and 4(c), changing the chemical potential μ (or the removal/addition of photons) gives rise to the soliton patterns [79,80]. Only the uniform density oscillation is seen, and no beats or soliton patterns appear in Fig. 4(b). The number of solitons increases as the photons are further added or removed. Meanwhile, the density oscillation becomes weak. In other words, starting with the SI phase and changing the chemical potential μ leads to a solitons + SF crossover instead of the SS phase. In the thermodynamic limit, the crossover region vanishes, and the system experiences first-order transitions immediately.

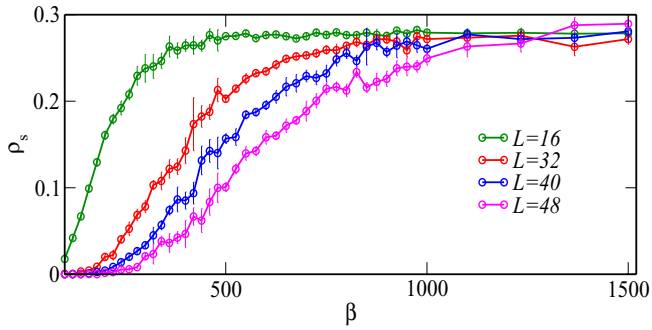

FIG. 5. Simulation results from the WQMC method of superfluid stiffness ρ_s as a function of β for the hard-core 1D JCH model. The parameters are $V/U = 0.4$, $\mu/U = -1$, and $t/U = 0.05$, and the system sizes are $L = 16$, 32, 40, and 48.

At the end of this section, the value of β is discussed. Usually, for the BH model, the ground state is reached if $\beta t > L$. For the JCH model, through careful checking, β should be much larger than L/t. In particular, for $L = 48$, ρ_s should reach convergence here at $\beta = 48/0.05 \approx 1000$. However, as shown in Fig. 5 with $L = 16$, 32, 40, and 48, the temperature should be sufficiently low enough for a ground state. Therefore, in this section, β is chosen to be 1500.

C. Hard-core JCH model on square lattice

Although the square lattice is a bipartite lattice, the physics between the 1D and 2D models may be different. To verify this, we still need to perform comprehensive WQMC simulations on the 2D geometries. Various global phase diagrams in the CMF frame were shown in Ref. [40].

As shown in Fig. 6, we also set t at the fixed value $t/U = 0.025$ and then measure ρ, $S(\mathbf{Q})/N$, and ρ_s as a function of μ/U. In a manner similar to that of the 1D model, we still see the SI phase (0,1,0,1) order in both directions, and the wave vector is $\mathbf{Q} = (\pi, \pi)$ in the range of $-1.960 < \mu/U < -1.698$, with signatures $\rho = 0.5$, $S(\mathbf{Q})/N \neq 0$, and $\rho_s = 0$. At the two ends of the SI phase, $S(\mathbf{Q})/N$ and ρ_s change discontinuously, which clearly indicates that no SS phase exists in the square lattices.

The histogram for $S_T(\mathbf{Q})/N$ obtained at the phase transition point in Fig. 6(d) shows two peaks which indicate the first-order transition between the SI and SF phases. Here, the total structure factor $S_T(\mathbf{Q})/N$ is defined by replacing n_i^a with $n_i^\sigma + n_i^a$ as a signature of the double peaks and is thus more clear.

IV. RESULTS FOR THE JCH MODELS ON TRIANGULAR LATTICES

A. Phase diagram and scanning the cut

The BH model on triangular lattices has been studied extensively [81–86]. Figure 7 shows the phase diagram obtained from the CMF method, which contains the empty, SII, SIII, MI ($\rho = 1$), SS, and SF phases in the plane $(t/U, \mu/U)$. The colored symbols denote the numerical results obtained by the WQMC method. The phase diagram of the pure BH model on triangular lattices has been obtained [81,82] and is symmetric

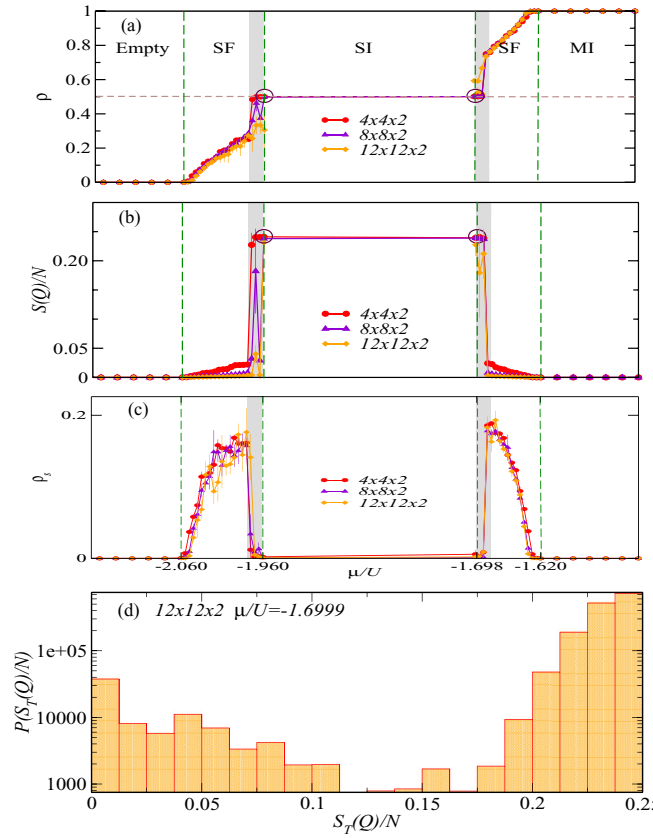

FIG. 6. Simulation results from the WQMC method for (a) ρ, (b) $S(\mathbf{Q})/N$, and (c) ρ_s as a function of μ/U for the JCH model on the square lattices. The parameters are $t/U = 0.025$, $\beta = 1000$, with $L = 4$, 8, 12. Dashed regimes are for first-order transitions. (d) Histogram of $S_T(\mathbf{Q})/N$ obtained at the phase transition point $\mu/U = -1.6999$ for system size $L = 12$.

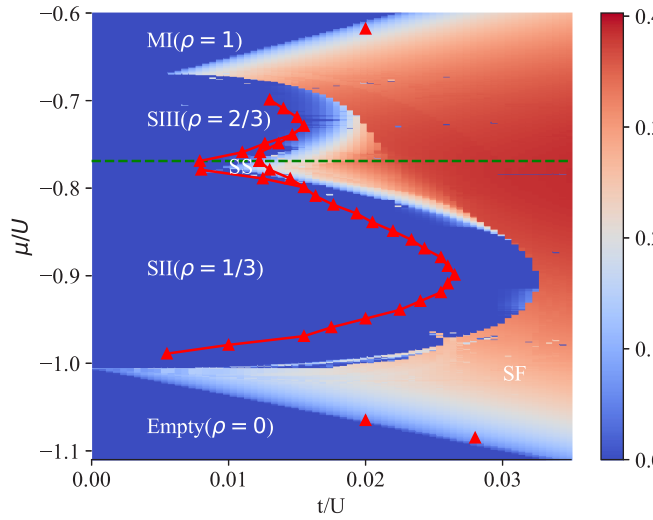

FIG. 7. The triangular lattice phase diagram and a detailed description of Ψ for the 2D JCH model with $V/U = 0.4$ by the CMF method. The red triangles are the phase boundaries given by the WQMC method, and the green dashed line labels the cut scanning with $\mu/U = -0.77$.

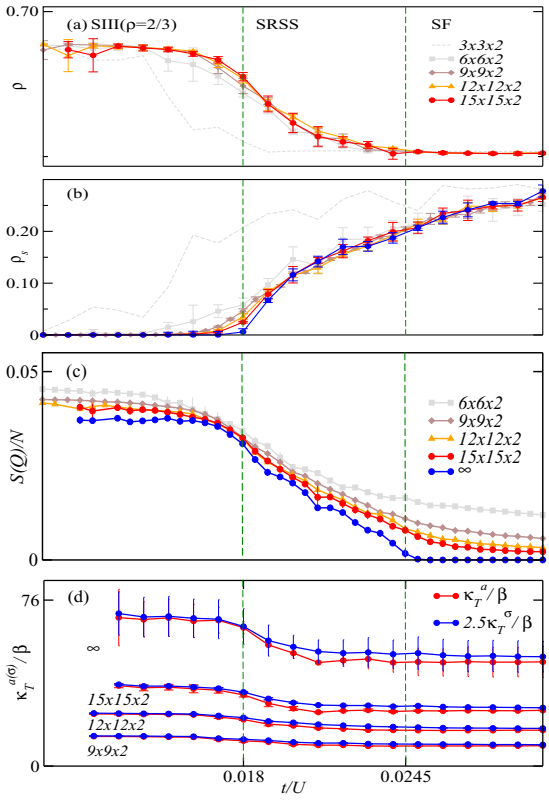

FIG. 8. Simulation results from the WQMC method for (a) ρ, (b) $S(Q)/N$, (c) ρ_s, and (d) $\kappa_T^{a(\sigma)}/\beta$ as a function of t/U for the JCH model on triangular lattices. The parameters are $\mu/U = -0.77$, $\beta = 500$, and the system sizes are $L \times L \times 2$, where $L = 6$, 9, 12, and 15.

about the particle-hole symmetric point $\mu/V = 3$. Here, for the JCH model, the phase diagram is not symmetric due to the atom-photon coupling, and a similar symmetric point can be found between the SII and SIII phases, which locates itself at about $\mu/U = -0.775$ (green dashed line) via the WQMC method. In a manner similar to that of the pure BH model, the solid-SF transition is first order, and the SF-MI transitions are continuous. Surrounded by the two types of solid phases and the SF phase, the SS phase emerges in the closed regime illustrated by lines with triangles, as shown in Fig. 7.

Figure 8 shows the WQMC simulations for ρ, ρ_s, $S(\mathbf{Q})/N$, and $\kappa_T^{a(\sigma)}/\beta$ as a function of t/U. In the regimes of $t/U < 0.018$, the systems are trapped in the SIII ($\rho = 2/3$) solid phase, with a signature of $S(\mathbf{Q})/N \neq 0$ and $\rho_s = 0$. When t/U increases, induced vacancies lead to the decrease from the excitation density, and both $S(\mathbf{Q})/N$ and ρ_s are nonzero. In particular, in the region of $0.018 \leqslant t/U \leqslant 0.0245$, the system sits in the SS phase stably in some special parameter regime of the triangular JCH model.

In Fig. 8(d), the nonzero $\kappa_T^{a(\sigma)}$ in the whole plotted regime means that the SF, solid, and SS phases possess the superradiant property; namely, the SS phase is actually a SRSS phase.

B. $S(\mathbf{Q})/N$ and $n(\mathbf{Q})$

Examples of the structure factor are shown in Figs. 9(a) and 9(b), with $L = 6$ and 12, respectively. The two peaks of $S(\mathbf{Q})/N$ with the maximum value are located at (0,0) because

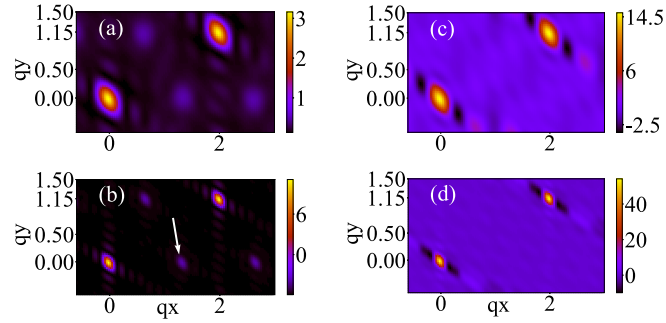

FIG. 9. Distribution of $S(qx, qy)$ and momentum distribution $n(qx, qy)$ for the SRSS phase on triangular lattices of size $L \times L \times 2$. (a) $S(qx, qy)$, $L = 6$. (b) $S(qx, qy)$, $L = 12$. (c) $n(qx, qy)$, $L = 6$. (d) $n(qx, qy)$, $L = 12$. The parameters are $\mu/U = -0.77$, $\beta = 500$, $t/U = 0.015$.

of a partial translational invariance of the densities on lattices. In the SRSS phase at $\mu/U = -0.77$, $t/U = 0.015$, we observe a second maximum at $\mathbf{Q} = (4/3\pi, 0)$, with a $\sqrt{3} \times \sqrt{3}$ diagonal long-range order of 2/3 filling [81,82]. This peak indicates the presence of a density ordering in the liquid phase, which defines a SRSS phase. The momentum distribution in Eq. (5) is also obtained as well as observed experimentally. The two peaks of $n(qx, qy)$ with maximum values are located at (0,0), which is a sign of the SF phase, as shown in Figs. 9(c) and 9(d).

C. The SRSS phase and the phase transitions

In the hard-core BH model on triangular lattices, it has been verified that the SS-SF transition type is continuous or first order, depending on the regimes of the chosen μ at the "symmetry point" or deviation away from the symmetry point, respectively [87,88].

In Fig. 10, we carefully examine the phase transitions among the SII, SRSS, and SF phases, with respect to the deviation from the symmetry point, i.e., the dashed line in Fig. 7. When $\mu/U = -0.78$ (pink line with circles) in Fig. 10(c), the first-order phase transition occurs between the SII and SRSS phases, confirmed by the bimodal distribution of total structural factors $S_T(\mathbf{Q})/N$ in Fig. 10(d). This kind of phase transition has not been reported for the pure BH model.

Simultaneously, the transition from the SRSS phase to the SF phase is first order at $\mu/U = -0.80$, as there is an obvious jump of $S(\mathbf{Q})/N$ at $t/U = 0.031$ [see the red line in Fig. 8(c)]. However, the transition is still continuous when $\mu/U = -0.78$ and -0.79, the same as the case with $\mu/U = -0.77$.

V. EXPERIMENTAL REALIZATION

The important experimental realization of the extended JCH model consists of inducing the interaction between photons or atom excitations, while the interaction between atom excitations could induce decoherence [89]. Fortunately, as shown in Fig. 11, Ref. [90] proposed that the cross-Kerr interaction between photons can be realized by the coupling between qubit 1 (blue box) and adjacent photon resonators (red balls). Qubit 2 (green box) is inserted by us for the

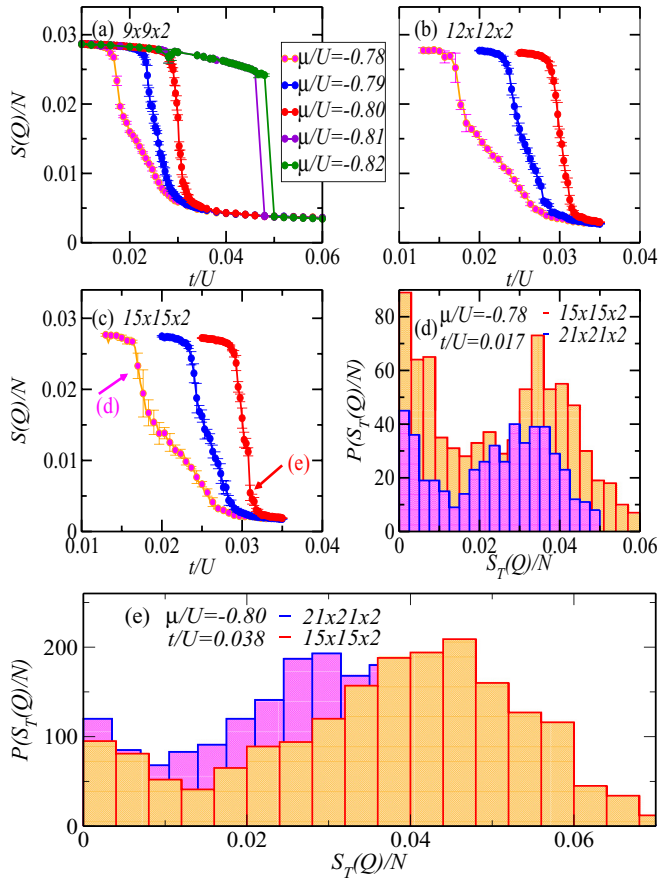

FIG. 10. Simulation results from the WQMC method for $S(\mathbf{Q})/N$ as a function of t/U for the JCH model on triangular lattices with parameter $\beta = 500$; the fixed sizes are (a) $L = 9$, (b) $L = 12$, and (c) $L = 15$. The colored lines denote different values of μ/U near the phase. (d) Histogram of $S_T(\mathbf{Q})/N$ obtained at the phase transition point $\mu/U = -0.78$ and $t/U = 0.017$ for system sizes $L = 15$ (orange) and 21 (purple). (e) Histogram of $S_T(\mathbf{Q})/N$ obtained at the phase transition point $\mu/U = -0.80$ and $t/U = 0.038$ for system sizes $L = 15$ (orange) and 21 (purple).

purpose of light-matter coupling according to Ref. [91]. This qubit is a superconducting Josephson junction, and it can act as a two-level atom [89].

With the basic resonator parameters C and L, the basic qubit parameters, i.e., capacitance C_J and Josephson energy E_J, and the resonator-qubit mutual capacitance C_g, one can estimate the experimental realizable parameters for the extended JCH model.

The coupling between the resonator (photon) and qubit (atom) is

$$U = \frac{C_g}{C_\Sigma} e V_{rms} \left(\frac{E_J}{2E_C^U} \right)^{\frac{1}{4}}, \tag{7}$$

where $C_\Sigma = C + C_J$, $V_{rms} = \sqrt{\omega_0/C}$ is the rms voltage of the vacuum field mode, and $\omega_0 = 1/\sqrt{LC}$ is the resonant frequency of the microwave photon. $E_C^U = \frac{e^2}{2(C_J + C_g)}$ is the charging energy of qubit 2, according to the parameters extracted from the work of Ref. [92] where the value of E_C^U is about 0.4 GHz.

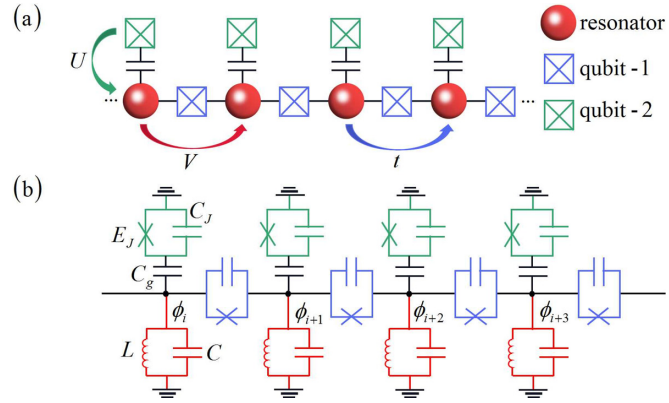

FIG. 11. (a) Schematic diagram of the experimental realization of the extended JCH model. The red ball is the photon resonator, the blue box is superconducting qubit 1, and the green box is superconducting qubit 2. (b) Effective circuit diagram of the system. The green qubit with capacitance C_J and Josephson energy E_J is matched to the resonator by a comparably large gate capacitance C_g. Qubit 1 (blue) with the same C_J and E_J connects two resonators (red) which are represented by the inductor L and capacitor C.

The cross-Kerr interactions between photons [90] can be described as

$$V = -\frac{2C_J}{\tilde{C}} E_C^V,$$

where $E_C^V = e^2/(2\tilde{C})$ is the charging energy of the nonlinear element (qubit 1) and $\tilde{C} = C_1 + 2C_J$, $1/\tilde{L} = 1/(2L_1) + 1/L_J$. C_1 and L_1 are modified symbols of C and L, respectively. Because when the photon resonator is coupled to qubit 2, the basic resonant frequency of photons ω_0 changes and can be modified to be $\omega_1 = \omega_0(1 + \frac{C_g^2}{C(C_J + C_g)}) = 1/\sqrt{L_1 C_1}$. Although it is attractive ($V < 0$), the system could still get nonuniform photon solids [93].

The hopping term [90] is described as

$$t = \omega_2 \Gamma,$$

with $\omega_2 = 1/\sqrt{\tilde{L}\tilde{C}}$ and $\Gamma = \frac{2L_1}{2L_1 + L_J} - \frac{C_J}{C_1 + 2C_J}$.

VI. CONCLUSION AND DISCUSSION

In conclusion, beyond the superradiant properties in the single-cavity system [36–38], we have theoretically investigated the hard-core JCH model on various lattices of cavity arrays using the large-scale WQMC method. Through the measurement of ρ, $S(Q)/N$, ρ_s, and $\kappa_T^{a(\sigma)}/\beta$, for a bipartite lattice such as the one-dimensional chain and square lattices, the previously found SS phase [40] is not reasonable.

We proposed the existence of the SRSS phase and found that it exists on triangular lattices. Different from the pure BH models, the (1/3)-filled solid (SII)-SRSS transition can be obviously first order, depending on the regimes of μ chosen.

The possible CQED realization of the SRSS phase has great advantages as the experiment can be easily designed and synthesized artificially and duplicated to assemble large-scale quantum systems and the light can be guided or confined in optical fibers without cooling [18]. At the same time, the distance between the cavities is comparably large, which is

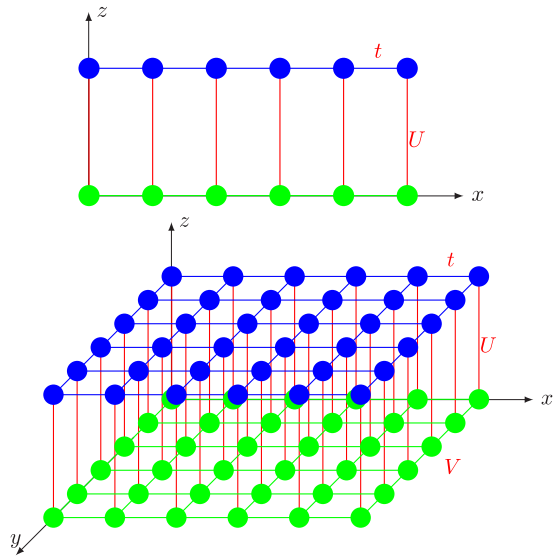

FIG. 12. The mapped two-layer one-dimensional chain and square lattices from the JCH model, where the top and bottom layers can be denoted as photon and atom layers, respectively. The hopping of photons t, atom-photon coupling U, and interactions between atom excitations V are labeled.

suitable for the manipulation and measurement of each cavity separately [20].

The results in this paper could stimulate the search for the new SRSS phase in circuit quantum electrodynamic experiments and other light-matter coupling systems.

ACKNOWLEDGMENTS

We thank Prof. N. V. Prokof'ev for sharing his codes with W.Z. during the 2017 Many Electron Collaboration Summer School held at the Simons Center at Stony Brook University. W.Z. is also grateful for the invaluable discussion on simulations with Z. Yao and L. Pollet. J.Z. is supported by the Open Project from the State Key Laboratory of Quantum Optics and Quantum Optics Devices in Shanxi Province (Grant No. KF201808). W.Z. is supported by NSFC under Grant No. 51901152. T.C.S. would like to thank M. Therani, principal of EngKraft LLC; S. Kanakakorn of BlockFint Thailand; K. Keshavamurthy of Sakha Global, Bangalore, India; and A. Lüchow of the Institut für Physikalische Chemie, RWTH Aachen University, for their support.

APPENDIX A: THE GEOMETRIES OF ONE-DIMENSIONAL CHAIN AND SQUARE LATTICES

In Fig. 12, we mapped the JCH model to a two-layer triangular lattice. Therein, we show the JCH model geometry of the one-dimensional chain and square lattices.

APPENDIX B: COMPARISON WITH EXACT DIAGONALIZATION

Before the large-scale simulations, we compare the results of small systems such as $L = 4$ using the WQMC method with ED for parameters $t/U = 0.05$ and $V/U = 0.4$ (Fig. 13). We

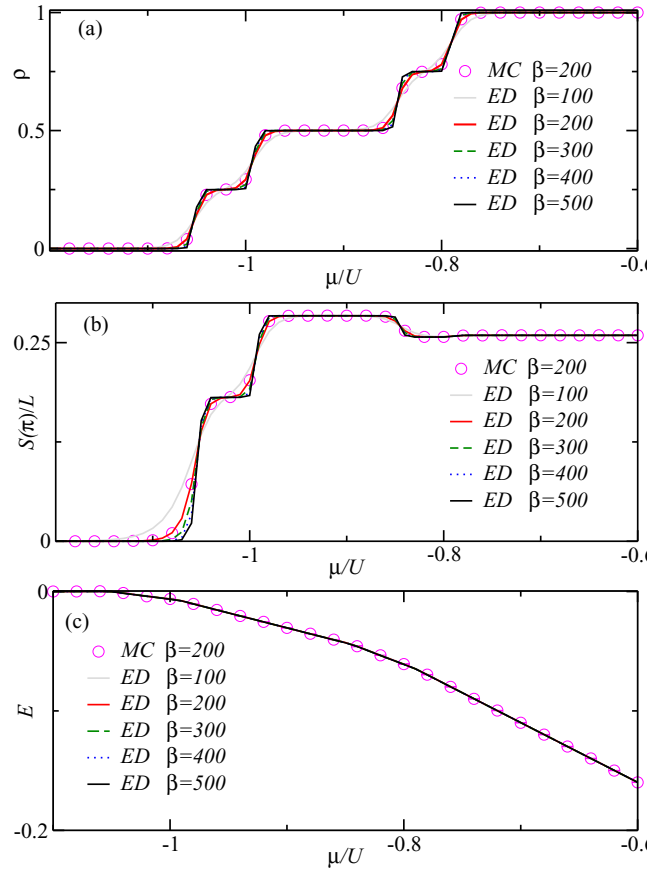

FIG. 13. Comparison of the simulation results of the one-dimensional JCH lattice with $L = 4$ from both the ED and WQMC methods for (a) ρ, (b) $S(\pi)/L$, and (c) E for various temperatures $\beta = 100$–500.

perform QMC at the fixed temperature $\beta = 200$, while ED is done with $\beta = 100, 200, 300, 400$, and 500. Quantities such as excitation densities ρ, the structural factors $S(\pi)/L$, and the energy densities E are shown and are consistent with each other.

APPENDIX C: CMF METHODS

In the CMF frame, the total Hamiltonian is taken to be $H_{tot} = H_{mf} + H_{ed}$, where the exactly treated H_{ed} is the Hamiltonian inside the cluster, such as the triangular lattice (ABC) illustrated in yellow in Fig. 14.

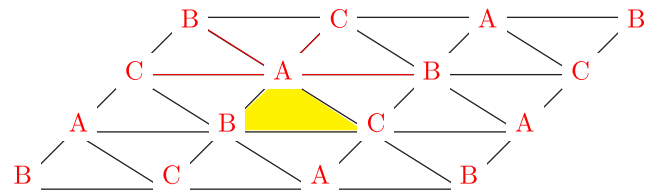

FIG. 14. A triangular lattice by three sublattices, A, B, and C. The triangle denoted in yellow is the cluster treated exactly. The interaction and hopping illustrated by the red lines such as AB and AC are decoupled approximately.

The Hamiltonian H_{mf} is given by

$$H_{mf} = -qt \sum_{i,j\in ce} [(a_i^\dagger + a_i)\Psi_j + (a_j^\dagger + a_j)\Psi_i - 2\Psi_i\Psi_j] + qV \sum_{i,j\in ce} \left(n_i^\sigma \rho_j^\sigma + n_j^\sigma \rho_i^\sigma - \rho_i^\sigma \rho_j^\sigma\right). \quad \text{(C1)}$$

Here, site A connects B and C by four red lines. Therefore, on average, q should be equal to 2 for triangular lattices. The symbol ce means sites along the edge of the yellow cluster. The symbol $\Psi_i = \langle a_i \rangle$ is the superfluid order parameter, and $\rho_i^\sigma = \langle n_i^\sigma \rangle$ is the number of atomic excitations.

TABLE I. Values of the order parameters for typical phases.

	Solid	SF	SS	MI
Ψ	0	$\neq 0$	$\neq 0$	0
$\Delta\Psi$	$\neq 0$	0	$\neq 0$	0
$\Delta\rho$	$\neq 0$	0	$\neq 0$	0

In practice, we determine the self-consistent solutions of ρ_i^σ and Ψ_i by iterative calculation of the ground state of the cluster system until the mean fields converge.

In Figs. 2 and 7, Ψ is plotted as background for the phase diagram (see Table I).

[1] O. Penrose and L. Onsager, Bose-Einstein condensation and liquid helium, Phys. Rev. **104**, 576 (1956).
[2] A. F. Andreev and I. M. Lifshitz, Quantum Theory of Defects in Crystals, Sov. Phys. JETP **29**, 1107 (1969).
[3] G. V. Chester, Speculations on Bose-Einstein condensation and quantum crystals, Phys. Rev. A **2**, 256 (1970).
[4] A. J. Leggett, Can a Solid Be "Superfluid"? Phys. Rev. Lett. **25**, 1543 (1970).
[5] M. Boninsegni and N. V. Prokof'ev, Colloquium: Supersolids: What and where are they? Rev. Mod. Phys. **84**, 759 (2012).
[6] M. H. W. Chan, R. B. Hallock, and L. Reatto, Overview on solid ^{4}He and the issue of supersolidity, J. Low Temp. Phys. **172**, 317 (2013).
[7] E. Kim and M. H. W. Chan, Probable observation of a supersolid helium phase, Nature (London) **427**, 225 (2004).
[8] J. Day and J. Beamish, Low-temperature shear modulus changes in solid ^{4}He and connection to supersolidity, Nature (London) **450**, 853 (2007).
[9] D. Y. Kim and M. H. W. Chan, Absence of Supersolidity in Solid Helium in Porous Vycor Glass, Phys. Rev. Lett. **109**, 155301 (2012).
[10] A. B. Kuklov, L. Pollet, N. V. Prokof'ev, and B. V. Svistunov, Quantum plasticity and supersolid response in helium-4, Phys. Rev. B **90**, 184508 (2014).
[11] J. Léonard, A. Morales, P. Zupancic, T. Esslinger, and T. Donner, Supersolid formation in a quantum gas breaking a continuous translational symmetry, Nature (London) **543**, 87 (2017).
[12] J. Li, J. Lee, W. Huang, S. Burchesky, B. Shteynas, F. Top, A. Jamison, and W. Ketterle, A stripe phase with supersolid properties in spin-orbit-coupled Bose-Einstein condensates, Nature (London) **543**, 91 (2017).
[13] L. Tanzi, E. Lucioni, F. Famà, J. Catani, A. Fioretti, C. Gabbanini, R. Bisset, L. Santos, and G. Modugno, Observation of a Dipolar Quantum Gas with Metastable Supersolid Properties, Phys. Rev. Lett. **122**, 130405 (2019).
[14] F. Böttcher, J. N. Schmidt, M. Wenzel, J. Hertkorn, M. Guo, T. Langen, and T. Pfau, Transient Supersolid Properties in an Array of Dipolar Quantum Droplets, Phys. Rev. X **9**, 011051 (2019).
[15] L. Chomaz, D. Petter, P. Ilzhöfer, G. Natale, A. Trautmann, C. Politi, G. Durastante, R. M. W. van Bijnen, A. Patscheider, M. Sohmen, M. J. Mark, and F. Ferlaino, Long-Lived and Transient Supersolid Behaviors in Dipolar Quantum Gases, Phys. Rev. X **9**, 021012 (2019).
[16] S. Ornes, The return of supersolids, Phys. World **30**, 24 (2017).
[17] I. Carusotto and C. Ciuti, Quantum fluids of light, Rev. Mod. Phys. **85**, 299 (2013).
[18] R. J. Schoelkopf and S. M. Girvin, Wiring up quantum systems, Nature (London) **451**, 664 (2008).
[19] J. Q. You and F. Nori, Atomic physics and quantum optics using superconducting circuits, Nature (London) **474**, 589 (2011).
[20] J. Kasprzak, M. Richard, S. Kundermann, A. Baas, P. Jeambrun, J. M. J. Keeling, F. M. Marchetti, M. H. Szymańska, R. André, J. L. Staehli, V. Savona, P. B. Littlewood, B. Deveaud, and L. S. Dang, Bose-Einstein condensation of exciton polaritons, Nature (London) **443**, 409 (2006).
[21] M. J. Hartmann, F. Brandão, and M. B. Plenio, Strongly interacting polaritons in coupled arrays of cavities, Nat. Phys. **2**, 849 (2006).
[22] A. D. Greentree, C. Tahan, J. H. Cole, and L. C. L. Hollenberg, Quantum phase transitions of light, Nat. Phys. **2**, 856 (2006).
[23] F. Deppe, M. Mariantoni, E. P. Menzel, A. Marx, S. Saito, K. Kakuyanagi, H. Tanaka, T. Meno, K. Semba, H. Takayanagi, E. Solano, and R. Gross, Two-photon probe of the Jaynes-Cummings model and symmetry breaking in circuit QED, Nat. Phys. **4**, 686 (2008).
[24] J. Koch and K. L. Hur, Superfluid-Mott-insulator transition of light in the Jaynes-Cummings lattice, Phys. Rev. A **80**, 023811 (2009).
[25] D. Underwood, W. Shanks, J. Koch, and A. Houck, Low-disorder microwave cavity lattices for quantum simulation with photons, Phys. Rev. A **86**, 023837 (2012).
[26] M. J. Hartmann, F. Brandão, and M. B. Plenio, Quantum many-body phenomena in coupled cavity arrays, Laser Photonics. Rev. **2**, 527 (2008).
[27] S. Schmidt, G. Blatter, and J. Keeling, From the Jaynes-Cummings-Hubbard to the Dicke model, J. Phys. B **46**, 224020 (2013).
[28] G. Kulaitis, F. Krüger, F. Nissen, and J. Keeling, Disordered driven coupled cavity arrays: Nonequilibrium stochastic mean-field theory, Phys. Rev. A **87**, 013840 (2013).
[29] C. Nietner and A. Pelster, Ginzburg-Landau theory for the Jaynes-Cummings-Hubbard model, Phys. Rev. A **85**, 043831 (2012).

[30] S. Schmidt and G. Blatter, Strong Coupling Theory for the Jaynes-Cummings-Hubbard Model, Phys. Rev. Lett. **103**, 086403 (2009).

[31] A. L. C. Hayward, A. M. Martin, and A. D. Greentree, Fractional Quantum Hall Physics in Jaynes-Cummings-Hubbard Lattices, Phys. Rev. Lett. **108**, 223602 (2012).

[32] G. Almeida and A. Souza, Quantum transport with coupled cavities on an Apollonian network, Phys. Rev. A **87**, 033804 (2013).

[33] Y. L. Dong, S. Q. Zhu, and W. L. You, Quantum-state transmission in a cavity array via two-photon exchange, Phys. Rev. A **85**, 023833 (2012).

[34] J. Quach, Disorder-correlation-frequency-controlled diffusion in the Jaynes-Cummings-Hubbard model, Phys. Rev. A **88**, 053843 (2013).

[35] M. Hohenadler, M. Aichhorn, S. Schmidt, and L. Pollet, Dynamical critical exponent of the Jaynes-Cummings-Hubbard model, Phys. Rev. A **84**, 041608(R) (2011).

[36] Y. Chen, Z. H. Yu, and H. Zhai, Quantum phase transitions of the Bose-Hubbard model inside a cavity, Phys. Rev. A **93**, 041601(R) (2016).

[37] X. F. Zhang, Q. Sun, Y. C. Wen, W. M. Liu, S. Eggert, and A. C. Ji, Superradiant Solid in Cavity QED Coupled to a Lattice of Rydberg Gas, Phys. Rev. Lett. **110**, 090402 (2013).

[38] Y. Chen, Z. H. Yu, and H. Zhai, Superradiance of Degenerate Fermi Gases in a Cavity, Phys. Rev. Lett. **112**, 143004 (2014).

[39] D. Jaksch, C. Bruder, J. I. Cirac, C. W. Gardiner, and P. Zoller, Cold Bosonic Atoms in Optical Lattices, Phys. Rev. Lett. **81**, 3108 (1998).

[40] B. Bujnowski, J. Corso, A. Hayward, J. Cole, and A. Martin, Supersolid phases of light in extended Jaynes-Cummings-Hubbard systems, Phys. Rev. A **90**, 043801 (2014).

[41] D. van Oosten, P. van der Straten, and H. T. C. Stoof, Quantum phases in an optical lattice, Phys. Rev. A **63**, 053601 (2001).

[42] D. Yamamoto, Correlated cluster mean-field theory for spin systems, Phys. Rev. B **79**, 144427 (2009); D. Yamamoto, G. Marmorini, and I. Danshita, Microscopic Model Calculations for the Magnetization Process of Layered Triangular-Lattice Quantum Antiferromagnets, Phys. Rev. Lett **114**, 027201 (2015).

[43] D. Lühmann, Cluster Gutzwiller method for bosonic lattice systems, Phys. Rev. A **87**, 043619 (2013).

[44] L. Guo, S. Greschner, S. Zhu, and W. Zhang, Supersolid and pair correlations of the extended Jaynes-Cummings-Hubbard model on triangular lattices, Phys. Rev. A **100**, 033614 (2019).

[45] S. R. White, Density Matrix Formulation for Quantum Renormalization Groups, Phys. Rev. Lett. **69**, 2863 (1992).

[46] U. Schollwöck, The density-matrix renormalization group, Rev. Mod. Phys. **77**, 259 (2005).

[47] The idea is from Prof. Lode Pollet.

[48] N. V. Prokof'ev, B. V. Svistunov, and I. S. Tupitsyn, "Worm" algorithm in quantum Monte Carlo simulations, Phys. Lett. A **238**, 253 (1998).

[49] L. Pollet, S. M. A. Rombouts, K. Van Houcke, and K. Heyde, Optimal Monte Carlo updating, Phys. Rev. E **70**, 056705 (2004).

[50] S. Rombouts, K. V. Houcke, and L. Pollet, Loop Updates for Quantum Monte Carlo Simulations in the Canonical Ensemble, Phys. Rev. Lett. **96**, 180603 (2006).

[51] L. Pollet, Recent developments in Quantum Monte-Carlo simulations with applications for cold gases, Rep. Prog. Phys. **75**, 094501 (2012).

[52] H. Matsuda and T. Tsuneto, Off-diagonal long-range order in solids, Prog. Theor. Phys. Suppl. **46**, 411 (1970).

[53] K. S. Liu and M. E. Fisher, Quantum lattice gas and the existence of a supersolid, J. Low Temp. Phys. **10**, 655 (1973).

[54] A. B. Kuklov and B. V. Svistunov, Counterflow Superfluidity of Two-Species Ultracold Atoms in a Commensurate Optical Lattice, Phys. Rev. Lett. **90**, 100401 (2003).

[55] C. Trefzger, C. Menotti, and M. Lewenstein, Pair-Supersolid Phase in a Bilayer System of Dipolar Lattice Bosons, Phys. Rev. Lett. **103**, 035304 (2009).

[56] J. P. Lv, Q. H. Chen, and Y. J. Deng, Two-species hard-core bosons on the triangular lattice: A quantum Monte Carlo study, Phys. Rev. A **89**, 013628 (2014).

[57] J.-Q. Liang, J.-L. Liu, W.-D. Li, and Z.-J. Li, Atom-pair tunneling and quantum phase transition in the strong-interaction regime, Phys. Rev. A **79**, 033617 (2009).

[58] X. F. Zhou, Y. S. Zhang, and G. C. Guo, Pair tunneling of bosonic atoms in an optical lattice, Phys. Rev. A **80**, 013605 (2009).

[59] Y. C. Wang, W. Z. Zhang, H. Shao, and W. A. Guo, Extended Bose-Hubbard model with pair hopping on triangular lattice, Chin. Phys. B **22**, 096702 (2013).

[60] C. Chung, S. Fang, and P. Chen, Quantum and thermal transitions out of the pair-supersolid phase of two-species bosons on a square lattice, Phys. Rev. B **85**, 214513 (2012).

[61] S. Guertler, M. Troyer, and F. Zhang, Quantum Monte Carlo study of a two-species bosonic Hubbard model, Phys. Rev. B **77**, 184505 (2008).

[62] A. J. R. Heng, W. Guo, A. W. Sandvik, and P. Sengupta, Pair hopping in systems of strongly interacting hard-core bosons, Phys. Rev. B **100**, 104433 (2019).

[63] Y. C. Chen, R. G. Melko, S. Wessel, and Y. J. Kao, Supersolidity from defect condensation in the extended boson Hubbard model, Phys. Rev. B **77**, 014524 (2008).

[64] L. Dang, M. Boninsegni, and L. Pollet, Vacancy supersolid of hard-core bosons on the square lattice, Phys. Rev. B **78**, 132512 (2008).

[65] H. P. Büchler and G. Blatter, Supersolid versus Phase Separation in Atomic Bose-Fermi Mixtures, Phys. Rev. Lett. **91**, 130404 (2003).

[66] I. Titvinidze, M. Snoek, and W. Hofstetter, Supersolid Bose-Fermi Mixtures in Optical Lattices, Phys. Rev. Lett. **100**, 100401 (2008).

[67] F. Karim Pour, M. Rigol, S. Wessel, and A. Muramatsu, Supersolids in confined fermions on one-dimensional optical lattices, Phys. Rev. B **75**, 161104(R) (2007).

[68] L. Seabra and N. Shannon, Supersolid Phases in a Realistic Three Dimensional Spin Model, Phys. Rev. Lett. **104**, 237205 (2010).

[69] D. Heidarian and A. Paramekanti, Supersolidity in the Triangular Lattice Spin-1/2 XXZ Model: A Variational Perspective, Phys. Rev. Lett. **104**, 015301 (2010).

[70] W. Han, X. Zhang, D. Wang, H. Jiang, W. Zhang, and S. Zhang, Chiral Supersolid in Spin-Orbit-Coupled Bose Gases with Soft-Core Long-Range Interactions, Phys. Rev. Lett. **121**, 030404 (2018).

[71] J. M. Fellows and S. T. Carr, Superfluid, solid and supersolid phases of dipolar bosons in a quasi-one-dimensional optical lattice, Phys. Rev. A **84**, 051602(R) (2011).
[72] A. W. Sandvik, Stochastic series expansion method with operator-loop update, Phys. Rev. B **59**, R14157 (1999).
[73] O. F. Syljuåsen and A. W. Sandvik, Quantum Monte Carlo with directed loops, Phys. Rev. E **66**, 046701 (2002).
[74] E. L. Pollock and D. M. Ceperley, Path-integral computation of superfluid densities, Phys. Rev. B **36**, 8343 (1987).
[75] G. G. Batrouni and R. T. Scalettar, Phase Separation in Supersolids, Phys. Rev. Lett. **84**, 1599 (2000).
[76] G. G. Batrouni, V. G. Rousseau, R. T. Scalettar, and B. Grémaud, Competing phases, phase separation, and coexistence in the extended one-dimensional bosonic Hubbard model, Phys. Rev. B **90**, 205123 (2014).
[77] P. Sengupta, L. P. Pryadko, F. Alet, M. Troyer, and G. Schmid, Supersolids versus Phase Separation in Two-Dimensional Lattice Bosons, Phys. Rev. Lett. **94**, 207202 (2005).
[78] M. Boninsegni, Phase Separation in Mixtures of Hard Core Bosons, Phys. Rev. Lett. **87**, 087201 (2001).
[79] T. Mishra, R. V. Pai, S. Ramanan, M. S. Luthra, and B. P. Das, Supersolid and solitonic phases in the one-dimensional extended Bose-Hubbard model, Phys. Rev. A **80**, 043614 (2009).
[80] W. Zhang, S. Greschner, E. Fan, T. C. Scott, and Y. Zhang, Ground state properties of the one-dimensional unconstrained pseudo-anyon Hubbard model, Phys. Rev. A **95**, 053614 (2017).
[81] S. Wessel and M. Troyer, Supersolid Hardcore Bosons on the Triangular Lattice, Phys. Rev. Lett. **95**, 127205 (2005).
[82] M. Boninsegni and N. Prokof'ev, Supersolid Phase of Hard-core Bosons on Triangular Lattice, Phys. Rev. Lett. **95**, 237204 (2005).
[83] W. Zhang, R. Yin, and Y. Wang, Pair supersolid with atom-pair hopping on the state-dependent triangular lattice, Phys. Rev. B **88**, 174515 (2013).
[84] T. Mishra, S. Greschner, and L. Santos, Polar molecules in frustrated triangular ladders, Phys. Rev. A **91**, 043614 (2015).
[85] D. Heidarian and K. Damle, Persistent Supersolid Phase of Hard-Core Bosons on the Triangular Lattice, Phys. Rev. Lett. **95**, 127206 (2005).
[86] R. G. Melko, A. Paramekanti, A. A. Burkov, A. Vishwanath, D. N. Sheng, and L. Balents, Supersolid Order from Disorder: Hard-Core Bosons on the Triangular Lattice, Phys. Rev. Lett. **95**, 127207 (2005).
[87] D. Yamamoto, I. Danshita, and C. A. R. Sá de Melo, Dipolar bosons in triangular optical lattices: Quantum phase transitions and anomalous hysteresis, Phys. Rev. A **85**, 021601(R) (2012).
[88] L. Bonnes and S. Wessel, Generic first-order versus continuous quantum nucleation of supersolidity, Phys. Rev. B **84**, 054510 (2011).
[89] M. J. Hartmann, Quantum simulation with interacting photons, J. Opt. **18**, 104005 (2016).
[90] J. S. Jin, D. Rossini, R. Fazio, M. Leib, and M. J. Hartmann, Photon Solid Phases in Driven Arrays of Nonlinearly Coupled Cavities, Phys. Rev. Lett. **110**, 163605 (2013).
[91] M. Leib and M. J. Hartmann, Bose-Hubbard dynamics of polaritons in a chain of circuit quantum electrodynamics cavities, New J. Phys. **12**, 093031 (2010).
[92] J. M. Fink, M. Göppl, M. Baur, R. Bianchetti, P. J. Leek, A. Blais, and A. Wallraff, Climbing the Jaynes-Cummings ladder and observing its $\sqrt{n}$ nonlinearity in a cavity QED system, Nature (London) **454**, 315 (2008).
[93] J. S. Jin, D. Rossini, M. Leib, M. J. Hartmann, and R. Fazio, Steady-state phase diagram of a driven QED-cavity array with cross-Kerr nonlinearities, Phys. Rev. A **90**, 023827 (2014).